Mapping the Impact of *DUSP6* in an ADHD iPSC derived-dopaminergic neuronal model

Atefeh Namipashaki[1], Shane D. Hellyer[2], Aurina Arnatkeviciute[1], Kevin Walsh[1], Cameron J Nowell[2], Jose M. Polo[3,4], Karen J Gregory[2], Mark A. Bellgrove[1], Ziarih Hawi[1]

1. Turner Institute for Brain and Mental Health, School of Psychological Sciences, Monash University, VIC, Australia
2. Drug Discovery Biology, Monash Institute of Pharmaceutical Sciences, Monash University, Parkville, VIC, 3052, Australia
3. Department of Anatomy & Developmental Biology, Monash University, Melbourne VIC 3800, Australia. Development and Stem Cells Program, Monash Biomedicine Discovery Institute, Melbourne VIC 3800, Australia. Australian Regenerative Medicine Institute, Monash University, Melbourne VIC 3800, Australia.
4. Adelaide Centre for Epigenetics and the South Australian Immunogenomics Cancer Institute, The University of Adelaide, SA, Australia

* The authors Ziarih Hawi and Mark Bellgrove contributed equally to this work and share last authorship

Correspondence
Dr Ziarih Hawi,
Turner Institute for Brain and
School of Psychological Sciences,
Monash Univesty, Clayton Campus,
Vic 3800
e–mail: ziarih.hawi@monash.edu

Abstract

Although the gene *DUSP6* has been implicated as a risk gene for ADHD in recent GWAS studies, its functional role in the aetiology of the condition remains poorly understood. *DUSP6* is reported to regulate dopaminergic neurotransmission by decreasing available synaptic dopamine, suggesting a potential mechanism by which *DUSP6* may confer risk to ADHD. In this study, we employed CRISPR-Cas9 to knockout *DUSP6* in induced pluripotent stem cells (iPSCs) derived from an individual with ADHD. These isogenic engineered cells were then differentiated into highly homogeneous dopaminergic neurons, including both heterozygous (Het) and homozygous (Hom) knockout lines, along with parental control lines, to assess changes in dopaminergic neurotransmission at both cellular and transcriptomic levels. Enzyme Linked Immunosorbent Assay (ELISA) analyses showed a dose-dependent trend of increasing dopamine levels, at extracellular level, in the knockout lines. RNA sequencing further supported this finding, showing that downregulation of *DUSP6* lead to the upregulation of differentially expressed genes (DEGs) associated with the regulation of dopamine secretion and synaptic functions critical for dopamine signalling. These DEGs appear to encode components of the synaptic machinery essential for effective dopamine transmission or act as regulators of dopaminergic neurotransmission. Additionally, RNA sequencing uncovered other potential biological mechanisms through which *DUSP6* may contribute to increase the risk for ADHD, including effects on neurogenesis, extracellular matrix-associated processes, lipid metabolism, and sex-specific gene expression. Furthermore, we identified overlaps between *DUSP6* knockout DEGs and those associated with other neuropsychiatric disorders, including major depression (MDD), bipolar disorder (BD), and schizophrenia (SCZ), suggesting shared genetic pathways potentially influenced by *DUSP6*. Together, this study provides deeper insights into the molecular underpinnings of the role played by *DUSP6* in the genetic aetiology of ADHD and its broader implications across related neuropsychiatric conditions.

Key words

ADHD, *DUSP6* (*MKP3*), CRISPR knockout, Dopaminergic differentiation, Stem cell modelling, Transcriptomics, Dopamine signalling

Introduction

Dual Specificity Phosphatase 6 (*DUSP6*), also known as *MKP3*, has been identified as a risk gene for various mental and neurological conditions, including attention deficit hyperactivity disorder (ADHD) (Faraone et al., 2024). Recent large-scale genome-wide association studies (GWAS) have highlighted *DUSP6* as a significant risk gene associated with ADHD (Demontis et al., 2023; Demontis et al., 2019). However, the molecular mechanisms by which *DUSP6* contributes to ADHD risk remain incompletely understood.

DUSP6 is a member of the dual specificity protein phosphatase subfamily and encodes a protein that inactivates target kinases by dephosphorylating both phosphoserine/threonine and phosphotyrosine residues (Seternes, Kidger, & Keyse, 2019). Given its broad range of substrates, *DUSP6* plays a crucial role in modulating diverse cellular functions, including the regulation of dopaminergic neurotransmission. This is particularly relevant since dysregulation of dopamine has long been hypothesised as central to the aetiology of ADHD, with psychostimulant medications —effective in treating the disorder—working by modulating dopamine signalling and increasing synaptic dopamine availability (Faraone et al., 2024). Previous research has shown that *DUSP6* can reduce synaptic dopamine levels (Mortensen, 2013; Mortensen, Larsen, Prasad, & Amara, 2008). For example, increased expression of *DUSP6* in a rat neuroendocrine pheochromocytoma PC12 cell line has been shown to eliminate dopamine release by downregulating L-type calcium channel (*CACNA1C*) expression, thereby inhibiting dopamine release from large dense core vesicles and reducing synaptic dopamine (Mortensen, 2013). Another study utilizing both overexpression and shRNA knockdown strategies, demonstrated that DUSP6 stabilizes the primary dopamine transporter (SLC6A3, previously known as DAT1), at the cellular membrane, enhancing SLC6A3 activity and consequently decreasing dopamine availability in the synapse (Mortensen et al., 2008). These findings suggest that *DUSP6* may act as a risk gene by reducing synaptic dopamine levels, which is hypothesised as central to the aetiology of ADHD.

We therefore hypothesized that downregulating *DUSP6* in dopaminergic neurons derived from individuals with ADHD would be associated with increased synaptic dopamine levels. To test this hypothesis, we generated isogenic *DUSP6* knockout cellular models using CRISPR-Cas9 gene editing in an induced pluripotent stem cell (iPSC) line derived from an individual with ADHD, producing both Het and Hom knockout variants. These iPSCs were

then differentiated into highly homogeneous dopaminergic neurons; the cell type most relevant to ADHD in the brain (Faraone et al., 2024).

To characterize the impact of *DUSP6* knockout, we first performed RNA sequencing (RNA-Seq) on the isogenic neurons to assess the effects of the absence of *DUSP6* on dopaminergic neurotransmission and other processes relevant to ADHD aetiology. Next, we quantified intra- and extracellular dopamine concentrations to evaluate the influence of *DUSP6* knockout on dopamine neurotransmission at the cellular level. Furthermore, given that *DUSP6* overexpression is reported to downregulate *CACNA1C*, a key player in calcium-dependent dopamine exocytosis, we also conducted calcium imaging to determine whether *DUSP6* knockout neurons exhibited increased calcium influx. Our findings suggest a dose-dependent regulatory effect of the absence of *DUSP6*, leading to enhanced synaptic dopamine levels, thus offering potential mechanistic insights into the pathophysiology of ADHD.

Materials and Method

iPSC culture

An iPSC line derived from peripheral blood mononuclear cells (PBMC) of a male youth with ADHD was used in this study (Tong et al., 2019). The iPSC line was seeded on Biolaminin–521 (Biolamina, Cat#LN521) coated plates and maintained in StemFlex medium (Gibco, Cat#A3349401) for up to three passages to reach and adapt to a healthy state.

CRISPR guide RNA (gRNA) design

The Alt-R CRISPR-Cas9 CRISPR RNA (crRNA) selection tool from Integrated DNA Technology (IDT) (https://sg.idtdna.com/site/order/designtool/index/CRISPR_PREDESIGN) was used to design the gRNA targeting exon 1 of the *DUSP6* gene. Details the gRNA and primer sequences used to amplify the targeted and the top two potential off-target regions are provided in Supplementary Table 1.

CRISPR mediated gene editing

CRISPR engineering of the iPSC line was conducted using our previously published protocol, which enables the generation of homogeneous edited iPSC clones within two weeks (Namipashaki et al., 2023). In brief, equimolar amounts (1 μM) of gRNA oligonucleotides and the Cas9 enzyme were combined to assemble the ribonucleoprotein (RNP) CRISPR complex. To facilitate transfection, dissociated iPSC clusters (a total of 150,000 cells) were

mixed with the RNP complex and Lipofectamine Stem Transfection Reagent (Invitrogen, Cat#STEM00015) and seeded on a well of 24-well plate. After 48 hours of incubation, the iPSCs were sorted to isolate the positively transfected cells. These cells were then seeded as single cells into individual wells of a 96-well plate and incubated for up to 10 days to allow for the growth and formation of single-cell clones. These single-cell clones were subsequently subjected to sanger sequencing to screen for the desired edited clones.

Western blotting

Western blotting was performed to confirm the Het and Hom knockout of DUSP6. Proteins were extracted from iPSCs using M-PER Mammalian Protein Extraction Reagent (Thermo Scientific, Cat#78501) supplemented with Halt Protease and Phosphatase Inhibitor Cocktail (Thermo Scientific, Cat#78440). The lysates were incubated on ice for 15 minutes, followed by centrifugation at 15,000 g for 15 minutes at 4°C. The supernatant was then collected, and protein concentration was determined using the Qubit Protein Assay Kit (Thermo Scientific, Cat#A50668).

For separation, protein extract was run on NuPAGE Bis-Tris protein gels (Invitrogen, Cat#NP0335BOX) alongside a Spectra Multicolor Broad Range Protein Ladder (Thermo Scientific, Cat#22623). Separated proteins were transferred onto a PVDF membrane (Invitrogen, Cat#IB24002). The membrane was blocked with 5% non-fat dry milk and incubated overnight with the primary antibody (Abcam, Cat#ab76310). After washing, the membrane was incubated with the appropriate secondary antibody (Abcam) for 1 hour. Detection was performed using the ECL Prime Western Blotting System (Cytiva, Cat#RPN2232) and imaged using the ChemiDoc system (Bio-Rad).

Dopaminergic neuron differentiation

Each cell line— the parental control, Het, and Hom—was differentiated into dopaminergic neurons in triplicate for all subsequent analyses. Differentiation was performed using a lentiviral induction method (Powell et al., 2023). In this approach, iPSCs were differentiated by culturing with a lentiviral system that inducibly expresses three transcription factors (ASCL1, LMX1B, and NURR1) alongside an antibiotic resistance gene (PuroR). The cells were cultured on plates coated with Biolaminin 111 LN (Biolamina, Cat#LN111) in a DMEM/F12-based medium (Gibco, Cat#10565018) supplemented with doxycycline (Sigma, Cat#D9891) to activate the transcription factors. Puromycin (Sigma, Cat#7255) was added to select cells that successfully incorporated the transgenes. At day 14 of in vitro differentiation

(DIV 14), the medium was replaced with BrainPhys (Stem Cell Technologies, Cat#05790) supplemented with growth factors and maintained until the cells matured into dopaminergic neurons, at DIV 35.

Immunocytochemistry

To confirm the dopaminergic identity of the generated neurons, we evaluated the expression of key dopaminergic markers, including tyrosine hydroxylase (TH), the rate-limiting enzyme in dopamine synthesis, and microtubule-associated protein 2 (MAP2), a reliable neuron-specific somatodendritic marker. On day 35, the culture medium was removed, and the neurons were washed twice with phosphate-buffered saline (PBS). The cells were then fixed with 4% paraformaldehyde (Electron Microscopy Sciences, Cat#15170) for 15 minutes, followed by three PBS washes and a 5-minute incubation in permeabilization buffer (0.5% Triton X-100, Sigma, Cat#T8787). After three more PBS washes, the neurons were blocked for 30 minutes in blocking buffer (3% BSA, Sigma, Cat#A7906). The cells were subsequently incubated with primary antibodies—Recombinant Anti-Tyrosine Hydroxylase (Abcam, Cat#ab75875) and Anti-MAP2 (Abcam, Cat#ab92434)—for 2 hours at 37°C. Following three PBS washes, the neurons were incubated with appropriate secondary antibodies (Abcam, Cat#ab150081, Cat#ab150174) for 1 hour at 37°C. After two PBS washes, a final last wash contained NucBlue Live Cell Stain (Thermo, Cat#R37605) was performed. The neurons were then immediately imaged using the EVOS M5000 Imaging System (Thermo Fisher Scientific).

RNA isolation, library preparation, and sequencing

RNA samples were isolated using TRIzol reagent (Thermo Fisher Scientific, Cat#15596026) and further purified with the RNeasy Kit (Qiagen, Cat#74104). Quantification, quality control, library preparation and sequencing of RNA samples were performed at the Australian Genome Research Facility (AGRF). After initial quality control checks to ensure of the quantity and integrity of the samples (Supplementary Table 2), 100 nanograms (ng) of RNA from each sample were used for sequencing. The RNA library was prepared using the Illumina Ribo-Zero Plus whole-transcriptome sequencing workflow, which includes an initial ribosomal RNA (rRNA) depletion step. Following rRNA depletion, the remaining RNA molecules were fragmented into 150 base pairs (bp) and underwent first and second cDNA synthesis via reverse transcription. The resulting cDNA samples were indexed through adapter ligation and amplified by PCR to produce the RNA sequencing libraries. Finally, the

samples were sequenced using the Illumina NovaSeq X Plus System, achieving a sequencing depth of 50 million reads per sample.

RNA-seq data processing and differential gene expression analysis

The automated nf-core/rnaseq bioinformatics pipeline was employed to process the paired-end reads obtained from RNA sequencing (Harshil Patel, 2023). Initially, Trim Galore v0.6.7 was used to trim adapters and remove low-quality reads from the raw sequencing data (Felix Krueger, 2021). The STAR aligner was then utilized to align and annotate the RNA sequences to the human reference genome GRCh38, using ENSEMBL version 109 gene annotations (Dobin et al., 2013). The aligned reads in BAM files were then converted to FASTQ format using Samtools v1.14 and subsequently merged with the unmapped reads (Patro, Duggal, Love, Irizarry, & Kingsford, 2017). Gene-level counts, normalized to account for transcript length, were generated using the Bioconductor package tximport (Soneson, Love, & Robinson, 2015). Differential gene expression analysis was carried out using the Degust web application, employing the limma-voom method (Law, Chen, Shi, & Smyth, 2014; Powell., 2019). DEGs with a false discovery rate (FDR) ≤ 0.05 were included in volcano plots for each pairwise comparison between parental, Het, and Hom lines. The top 10 DEGs were selected based on the highest significance according to FDR. The list of DEGs that exhibited consistent directional changes across Het, and Hom lines compared to the parental line was selected to represent the DEGs altered due to the dose effect of *DUSP6*, referred to as *DUSP6* dose-responsive DEGs.

Interaction network, clustering and enrichment analysis

We utilized the list of DEGs (FDR ≤0.05) from each pairwise comparison and the *DUSP6* Dose-Responsive DEGs for functional network analysis using the STRING database (Law et al., 2014; Szklarczyk et al., 2023). STRING is a resource and a software tool for exploring known and predicted protein-protein interactions, allowing for the investigation of functional associations between genes. The DEGs were first categorized based on upregulation or downregulation and then submitted to the STRING database (https://string-db.org/) to visualize the interaction networks (Law et al., 2014). Following this, the DEGs were clustered into groups based on their interactions, functional similarities, and shared pathways using the K-means clustering functions (Brohee & van Helden, 2006). Since the STRING database also provides enrichment analysis for each cluster, clusters were grouped and named based on the overarching theme of the enriched biological processes. Automated pathway enrichment analysis is performed by STRING by assigning genes to their corresponding

pathways, as annotated in The Gene Ontology (GO) resource (Gene Ontology et al., 2023). Pathways identified if they occurred more frequently than expected by chance, using hypergeometric testing. The enrichment strength is represented as the logarithmic ratio (Log10) of observed versus expected counts, where the observed value is the number of genes in the cluster annotated with a specific term, and the expected value represents the number of genes that would be annotated with this term in a random network of the same size. To assess statistical significance, p-values were calculated and adjusted for multiple testing within each category using the Benjamini–Hochberg procedure to control the false discovery rate (Szklarczyk et al., 2021).

Analysis of *DUSP6*-DEG overlap with GWAS identified genes for major psychiatric disorders

Given that *DUSP6* has also been reported as a risk locus for other psychiatric disorders, we examined the overlap of DEGs from each pairwise comparison of the parental, Het, and Hom lines with GWAS-identified genes for major psychiatric disorders, including ADHD, SCZ, MDD, BD, and autism spectrum disorder (ASD). The risk genes for each disorder were derived using the multi-marker analysis of genomic annotation (MAGMA) software package (de Leeuw, Mooij, Heskes, & Posthuma, 2015). SNPs were mapped to corresponding genes using the MAGMA software package (de Leeuw et al., 2015), with annotation files and the 1000 Genomes European ancestry reference panel for linkage disequilibrium (LD) downloaded from https://github.com/thewonlab/H–MAGMA. Gene analyses were conducted using a multiple linear principal component regression model, with gene p-values computed via F-test. Genes more significantly involved in GWAS were assigned lower p-values. We applied Bonferroni correction (p-value ≤ 0.05/total genes) to select significant genes for each GWAS, identifying 95 genes for ADHD, 336 for BD, 465 for MDD, 922 for SCZ, and 14 for ASD.

The correspondence between ADHD-DEGs and GWAS-implicated genes for each disorder was assessed by determining the number of ADHD-DEGs present in the GWAS-identified gene lists. The statistical significance of the overlap was evaluated through permutation testing, comparing the number of overlapping genes in the empirical data to an ensemble of 100,000 randomly selected gene lists of the same size as the GWAS-identified gene sets. The permutation-based approach estimates a p-value with a minimum resolution of 10^{-5} (corresponding to 1/100000). If the estimated p-value is lower, we conservatively place it at 10^{-5}. Overlapped genes for each disorder were subsequently analysed for their

overrepresentation in biological processes using The Gene Ontology resource (de Leeuw et al., 2015).

Dopamine ELISA measurement of intra- and extracellular dopamine

Intra and extracellular dopamine concentrations were quantified using ELISA. Media supernatants were first aspirated and flash–frozen in liquid nitrogen. The neurons were then imaged using the cell viability stain (Thermo# A15001) to calculate the area of viable cells. Subsequently, they were harvested using Accutase and spun at 1000 × g for five minutes at room temperature (RT). The supernatants were completely aspirated, and cell pellets were flash–frozen in liquid nitrogen. The ELISA assay was conducted using the Dopamine Research ELISA Kit (ALPCO, #17–DOPHU–E01–RES) according to the manufacturer's instructions. Cells were lysed by sonication using the Diagenode Bioruptor Plus, set to 10 cycles (30sec on, followed by 30sec off per cycle). Absorbance at 450 nm was measured on a CLARIOstar Plus Microplate Reader (BMG LABTECH). Dopamine concentrations of the samples were calculated using Microplate Reader data analysis Software (MARS) and were normalized to micromoles of dopamine per relative fluorescent unit (RFU) of viable cells (µMols/RFU).

Ca imaging

At DIV42, the culture media were half-changed twice with calcium assay buffer, prepared as follows: 10 % 10x HBSS, 2 % 1M HEPES, 1 % 100x CaCl2, and 1 % probenecid, adjusted to pH to 7.4. Neurons were then loaded with Fluo-8 dye (1.6 µM, diluted in calcium assay buffer) and incubated for 45 minutes at 37°C. Following two additional half-washes with calcium assay buffer, the neurons were imaged using an Instant Structured Illumination Microscope (ISIM). Calcium imaging was performed across five wells for each of the parental, Het, and Hom lines, to be able to record a minimum of 80 cells for each group. Neurons were imaged for a total duration of 90 seconds, which included approximately 45 seconds of baseline calcium influx recording and 43.5 seconds of evoked response recording, stimulated with 100 mM potassium chloride (KCl) buffer. The entire recording period was divided into epochs: baseline (-35 to -25 s), pre-stimulus (-25 to -5 s), stimulus onset (-5 to 8 s), and stimulus response (8 to 20 s).

The data were first normalized to the baseline period (-35 to -25 s) and converted from absolute fluorescence measurements to $\Delta F/F_0$, where F_0 represents the mean amplitude of each individual cell's activity during the baseline period (-35 to -25 s), and $\Delta F/F_0$ is the ratio

of the cell's amplitude at any given time point relative to its individual F_0. Statistical analysis was conducted using mixed-effects modelling in MATLAB.

Results

Generation of *DUSP6* heterozygous and homozygous knock-out dopaminergic lines

Using our previously published method which efficiently generates homogeneous single-cell CRISPR-edited clones, we successfully produced two single-cell clones with *DUSP6* knockouts (Namipashaki et al., 2023). One clone exhibited disruption of one allele (Het), while the other clone showed disruption of both alleles (Hom), as confirmed by Sanger sequencing (Figure 1A). Further in silico and in vitro analyses (using PHYRE2 protein structure prediction tool) confirmed the disruption of one allele in the Het clone and both alleles in the Hom clone. The PHYRE2 protein structure prediction tool revealed altered conformational structures in both the Het and Hom lines (Figure 1B), and western blotting confirmed the absence of DUSP6 protein in the knockout lines in a dose-dependent manner (Figure 1C) (Kelley, Mezulis, Yates, Wass, & Sternberg, 2015).

We then applied an induction-based differentiation protocol to the parental, Het, and Hom *DUSP6* knockout iPSC lines which resulted in highly homogeneous populations of dopaminergic neurons. These neurons expressed TH, a key immunohistochemical marker of dopaminergic neurons, with over 99% purity. Additionally, they expressed MAP2, a neuron-specific somatodendritic marker (Figure 1D).

Transcriptome analysis of knocked-out lines and biological clustering of DEGs

To investigate the gene expression changes associated with reduced *DUSP6* expression, we employed whole-transcriptome RNA sequencing followed by pairwise differential expression analysis between parental, Het, and Hom lines. The comparison between parental and Hom lines revealed 514 DEGs with a substantial effect size, characterized by a log2 fold change greater than 2. The top 10 DEGs in this group, ranked by FDR significance, included genes reported to be associated with neurogenesis and synaptic plasticity (*TNC*, *FSTL1*, *SEMA3C*, and *ANOS1*) or components of the brain extracellular matrix (*COL1A2*, *FKBP10*, *IGFBP7*, *FBN1*, *CDH6*, and *COL4A2*) (Figure 2A and Supplementary Table 3) (Arora, Yeliosof, & Chin, 2023; Barnes et al., 2012; Chen, Hui, & Li, 2024; Clay & Halloran, 2014; Kumari et al., 2023; Moreno-Flores et al., 2003; Sadick et al., 2022; Tucic, Stamenkovic, & Andjus, 2021; Zagaglia et al., 2018).

In the comparisons of Het vs. Hom and parental versus Het lines, we identified 77 and 25 DEGs with high effect sizes, respectively (Supplementary Tables 4–5). These genes shared functional overlap with those identified in the parental versus Hom comparison, particularly in neurogenesis (*TNC*, *SLITRK4*, *PIWIL2*, *CPC4*, and *FOXF2*) and extracellular matrix composition (*COL1A2*, *IGFBP7*, *CDH6*, and *FBN2*) in the Het vs. Hom comparison, and neurogenesis (*SLITRK4*, *ALG10*, *ZNF439*, *SLITRK2*, *CNTN4*, and *DPP10*) in the parental versus Het comparison (Chen et al., 2024; Chernousov et al., 2010; Clay & Halloran, 2014; Everson et al., 2017; Farhy-Tselnicker et al., 2017; Gasperini et al., 2023; Maffie & Rudy, 2008; Matsumoto et al., 2024; Prakash, 2022; Tucic et al., 2021). Additionally, some DEGs were implicated in dopaminergic neuron development and survival, such as *WLS* (Het versus Hom) and *CHL1* (parental versus Hom) (Alsanie, Penna, Schachner, Thompson, & Parish, 2017; Prakash, 2022). Interestingly, sperm-related genes, including *HSPA2* and *SOHLH2*, were also among the top 10 DEGs in the parental versus Het comparison (Nowicka-Bauer et al., 2022; Park et al., 2016).

We next identified the DEGs that showed consistent directional changes across the parental, Het, and Hom lines, representing DEGs altered due to the dose effect of *DUSP6*. These DEGs are referred to as *DUSP6* dose-responsive DEGs. A total of 2,352 *DUSP6* dose-responsive DEGs were identified, with 1,499 negatively regulated and 853 positively regulated (Figure 2B). The top 10 dose-responsive DEGs are all downregulated and include genes related to neurogenesis (TNC, FSTL1, SEMA3C, FLNA, and ANOS1), components of the brain extracellular matrix (COL1A2, FKBP10, IGFBP7, and FBN1), and the spermatogenesis-associated gene SPATS2L (Figure 2C) (Arora et al., 2023; Barnes et al., 2012; Chen et al., 2024; Kumari et al., 2023; Moreno-Flores et al., 2003; Sadick et al., 2022; Sheen et al., 2002; Tucic et al., 2021). The high level of shared functions among the top 10 genes from the pairwise comparisons and the dose-responsive DEGs underscores the critical role of *DUSP6* in regulating these processes in the brain, primarily through its dephosphorylation enzymatic activity (Seternes et al., 2019).

Biological clustering of DEGs

To analyse the absence of dephosphorylation activity of *DUSP6* on certain downstream brain functions/pathways, we first categorized the DEGs from each group of pairwise comparison, along with the *DUSP6* dose-responsive DEGs, into two classes: negatively regulated and positively regulated (Supplementary Table 6). Within each class, the DEGs were clustered based on their network interactions, functional similarities, and shared pathways using the

STRING database. The clusters were grouped and named based on the overarching theme of the enriched biological processes presented by STRING (Supplementary Table 7). Consequently, the negatively regulated DEGs were clustered into groups mainly involved in biological processes related to developmental processes (e.g. regulation of developmental process, GO:0050793, FDR = 1.18 x 10^{-36}), extracellular matrix organization, (e.g. extracellular matrix organization, GO:0030198, FDR = 2.08 x 10^{-37}), tissue morphogenesis/ anchoring junctions (e.g. regulation of actin filament-based process, GO:0032970, FDR = 2.56 x 10^{-7}), apoptosis (e.g. regulation of programmed cell death, GO:0043067, FDR = 1.67 x 10^{-41}), regulation of transcription (e.g. regulation of RNA metabolic process, GO:0051252, FDR = 3.56 x 10^{-17}), and organelle transport (e.g. Golgi vesicle transport, GO:0048193, FDR = 2.03 x 10^{-7}) (Figure 3A). Among these, clusters related to developmental processes and extracellular matrix organization were shared across all comparisons.

The positively regulated DEGs were clustered into sub-groups primarily associated with biological processes involved in synaptic neurotransmitter transport (e.g. Neurotransmitter transport, GO:0006836, FDR = 4.35 x 10^{-17}), neurogenesis (e.g. generation of neurons, GO:0048699, FDR = 1.05 x 10^{-6}), cilia/microtubule and cell projection (e.g. cilium organization, GO:0044782, FDR = 1.37 x 10^{-6}), lipid metabolism (e.g. cholesterol biosynthetic process, GO:0006695, FDR = 1.61 x 10^{-6}), and regulation of transcription (e.g. regulation of transcription, DNA-templated, GO:0006355, FDR = 1.17 x 10^{-21}) (Figure 3B). Notably, genes involved in synaptic neurotransmitter transport comprised a substantial portion of the DEGs in each comparison, accounting for over 40%. These DEGs were enriched in various synaptic related biological processes such as synapse assembly (GO:0007416, FDR = 4.45 x 10^{-8}), trans-synaptic signalling (GO:0099537, FDR = 1.44 x 10^{-39}), vesicle-mediated transport in synapse (GO:0099003, FDR = 2.66 x 10^{-14}), neurotransmitter secretion (GO:0007269, FDR = 1.63 x 10^{-14}) and synaptic transmission, dopaminergic (GO:0001963, FDR = 7.5 x 10^{-3}) . Similar to the top-ranked DEGs, the clustered DEGs indicate that DUSP6 has a wide-ranging modulatory influence on various cellular functions in the brain, by both up and down-regulation of its target gene, each representing a potential mechanism contributing to ADHD aetiology.

Dose-dependent regulatory effect of *DUSP6* on dopaminergic neurotransmission

To determine whether *DUSP6* knockout in dopaminergic neurons derived from individuals with ADHD could enhance dopaminergic neurotransmission, we measured dopamine concentrations at both intra and extracellular levels. We observed increasing trend in

dopamine concentration in both Het and Hom lines compared to the parental control line, with a more pronounced increase in extracellular dopamine levels. Specifically, extracellular dopamine was significantly higher in the parental vs Hom group ($p = 0.016$), though this significance did not survive multiple testing after Bonferroni correction (threshold p 0.008), (Figure 4A). To investigate if this trend was reflected in the transcriptome data, we selected two of top biological processes related to dopamine release—regulation of dopamine secretion (GO:0014059, FDR = 1.80×10^{-5}) and neurotransmitter transport (GO:0006836, FDR = 1.3×10^{-3})—from the parental vs. Hom comparison. We then modelled the expression levels of DEGs within these processes across the parental, Het, and Hom lines to illustrate expression trends influenced by the dosage-dependent regulation of DUSP6. We observed that the trend in dopamine concentration was consistent with the increased expression of DEGs enriched in these two biological processes across the parental, Het, and Hom lines (Figure 3B). For instance, in the 'regulation of dopamine secretion' process, SYT13 (Synaptotagmin 13) expression in the Hom line increased by 0.62-fold compared to the Het line and by 0.94-fold compared to the parental line (FDR = 1.85×10^{-4}). Similarly, in the 'neurotransmitter transport' process, NRXN2 (Neurexin-2) expression in the Hom line increased by 0.5-fold compared to the Het line and by 1.02-fold compared to the parental line (FDR = 8.93×10^{-4}).

Overlap of *DUSP6* knocked-out DEGs with other major psychiatric disorders

Given that *DUSP6* is also associated with other psychiatric conditions, we tested whether *DUSP6* DEGs from the pairwise comparisons between parental, Het, and Hom lines overlapped with GWAS-identified risk genes for major psychiatric disorders, including SCZ, MDD, BD, and ASD. The DEGs from the parental versus Hom comparison showed significant overlap with risk genes for BD (FDR = 7.0×10^{-5}), MDD, (FDR = 1.0×10^{-5}), and SCZ (FDR = 1.0×10^{-5}) (Figure 5A).

To further explore the biological significance of these overlaps, we analysed the overrepresentation of the overlapping DEGs in specific biological processes. The DEGs overlapping with BD risk genes were significantly overrepresented in processes related to the plasma membrane, cell periphery, and membrane as indicated by GO:0005886 (FDR = 1.02×10^{-2}), GO:0016020 (FDR = 1.02×10^{-2}), and GO:0071944 (FDR = 1.02×10^{-2}) (Figure 5B and Supplementary Table 8). The DEGs overlapping with SCZ risk genes showed significant enrichment in biological processes associated with neurogenesis and synapse organization, such as nervous system development (GO:0007399, FDR = 1.02×10^{-10}),

synapse organization (GO:0050808, FDR = 7.51×10^{-6}), and neuron differentiation (GO:0030182, FDR = 5.26×10^{-5}) (Figure 5C and Supplementary Table 9). Similarly, the DEGs overlapping with MDD risk genes were significantly enriched in processes related to neurogenesis, axon guidance, and synapse assembly, such as axon guidance (GO:0007411, FDR = 3.99×10^{-2}), synapse assembly (GO:0007416, FDR = 3.4×10^{-14}), and axonogenesis (GO:0007409, FDR = 1.18×10^{-2}) (Figure 5D and Supplementary Table 10). In contrast, DEGs from other pairwise comparisons, including parental versus Het and Het versus Hom, did not show nominal significance for overlap with risk genes of other psychiatric disorders after multiple correction.

Effect of *DUSP6* knockout on *CACNA1C* calcium channel in dopaminergic neurons

Given that *DUSP6* overexpression has been reported to downregulate *CACNA1C*, a gene critically involved in calcium channel regulation, we conducted calcium imaging to explore whether DUSP6 knockout neurons exhibited increased CACNA1C expression and a corresponding rise in calcium influx at both baseline and evoked levels. Our analysis involved comparing the parental, Het, and Hom lines to determine if the absence of *DUSP6* would lead to functional alterations in calcium dynamics. Contrary to our expectations, the data did not show significant differences across the parental, Het, and Hom lines in either baseline or evoked calcium amplitude, suggesting that the knockout of *DUSP6* does not markedly impact these aspects of calcium signalling (Figure 6A-B). Additionally, we assessed the frequency of spontaneously active cells to determine whether there was an increase in spontaneous calcium activity as a result of *DUSP6* knockout. Similar to the other measurement, we found no significant differences between the lines in the frequency of spontaneously active cells (Figure 6C). These findings are consistent with our gene expression data, which show that *CACNA1C* expression is not significantly altered due to the knockout of *DUSP6* in either the Het or Hom lines (Figure 6D).

Discussion

In this study we highlight the potentially role of the *DUSP6* gene in the pathophysiology of ADHD, specifically through its influence on dopaminergic neurotransmission. Our findings revealed a trend towards a dose-dependent regulatory effect of *DUSP6* on dopaminergic signalling, where the knockout of *DUSP6* led to increasing dopamine levels, at extracellular level. This was further supported by the upward trend in DEGs associated with processes related to the regulation of dopamine secretion and neurotransmitter transport, observed across our experimental lines. Our RNA-seq analysis suggests that the *DUSP6* knockout

primarily affects genes involved in synaptic functions that are crucial for dopaminergic transmission. These DEGs appear to either encode components of the synaptic machinery required for effective dopamine secretion or act as regulators of dopaminergic neurotransmission. This highlights the role of *DUSP6* in modulating the functional aspects of dopamine signalling at the synapse.

Our data indicate that *DUSP6* is not only a key regulator of dopaminergic neurotransmission but also a major modulator of various other cellular functions in the brain. The downregulated genes observed in our study are predominantly associated with neuronal structure and developmental processes, while the upregulated genes span a wide range of cellular functions, including neurogenesis, lipid metabolism, and cilium/spermatogenesis. Interestingly, a significant portion of the downregulated DEGs with high effect sizes are related to extracellular matrix associated (ECM) proteins, such as cadherins and collagens. This finding aligns with previous reports linking cadherin genes to ADHD, suggesting that one pathway through which *DUSP6* might contribute to ADHD development is by modulating the extracellular matrix (Hawi et al., 2018).

Moreover, the observed links between neurogenesis, apoptosis, and *DUSP6* may be explained by the role of *DUSP6* as a member of the Mitogen-Activated Protein Kinase Phosphatases (MKPs). MKPs are known to modulate cellular functions related to proliferation, differentiation, and apoptosis via the MAPK signalling pathways (Patterson, Brummer, O'Brien, & Daly, 2009). This suggests that *DUSP6* may influence ADHD pathophysiology through its broader regulatory effects on cellular development and survival. Additionally, our data showed enrichment of upregulated DEGs in lipid metabolism processes, particularly cholesterol biosynthesis. Cholesterol is a critical component of cell membranes and plays an essential role in brain development and function, including membrane fluidity and synaptogenesis (Koudinov & Koudinova, 2002; Linetti et al., 2010). Since cholesterol cannot cross the blood-brain barrier, the brain relies on its own synthesis (Yang et al., 2022). This production is crucial, particularly during brain development. (Yang et al., 2022). This suggests another potential mechanism by which *DUSP6* may contribute to ADHD—by modulating synaptic neurotransmission through the regulation of cholesterol biosynthesis.

Furthermore, we observed DEGs associated with sperm/cilium structure and function, which potentially aligns with previous reports of *DUSP6*'s sex-specific roles in the brain and its association with psychiatric conditions in a sex-specific manner, including major depression

and bipolar disorder (Labonte et al., 2017). The higher prevalence of ADHD in male compared to female children may be partly attributed to sex-specific DEGs associated with DUSP6. For example, the downregulation of *HSPA2* and *SOHLH2*—both key players in spermatogenesis and highly expressed in the male reproductive system (Park et al., 2016)—in *DUSP6* knockout dopaminergic neurons may indicate neurodevelopmental downstream pathways that are more sensitive in males. This provides a potential link between *DUSP6* expression and the observed gender disparity in ADHD prevalence (Ramtekkar, Reiersen, Todorov, & Todd, 2010).

The overlap of *DUSP6* knockout DEGs with those associated with other disorders, including major depression, bipolar disorder, and schizophrenia, suggests shared genetic pathways potentially driven by *DUSP6*. Downregulation of *DUSP6* expression has been reported in post-mortem brain tissue of patients with depressive disorders, as well as in those with bipolar disorder (Labonte et al., 2017; Struyf, Dobrin, & Page, 2008). Further, the increasing use of antipsychotic medications has been shown to downregulate *DUSP6* in the anterior cingulate cortex (ACC) of patients with schizophrenia, suggesting that *DUSP6* may have originally been upregulated in this disorder, and the antipsychotic medications may have targeted this gene, leading to its downregulation (Kondo et al., 2022). This indicates that both over- and under-regulation of *DUSP6* can lead to significant dysfunctions in key brain pathways, potentially contributing to the manifestation of these disorders.

Our study suggests that *DUSP6* may have differing regulatory effects on calcium channels depending on whether it is upregulated or downregulated. While upregulation of *DUSP6* has been shown to downregulate *CACNA1C*, our findings indicate that the reverse is not necessarily true (Mortensen, 2013). This discrepancy could be attributed to previous work been conducted in a rat PC12 adrenal medullary tumor-derived cell line, whereas our experiments were performed in a human dopaminergic neuronal model. This highlights the importance of considering different cell types and species, as they may have distinct regulatory networks, underscoring the importance to study disorders in a cell-type-specific context. To gain a deeper understanding, follow-up experiments using CRISPR activation (CRISPRa) and CRISPR interference (CRISPRi) in more complex models, such as organoids, are recommended to better understand the effect of both over and under expression of *DUSP6*.

Although extracellular dopamine levels showed an increasing trend, the result did not reach statistical significance after correction for multiple comparisons. Given this trend, it is possible that a larger sample size with greater statistical power or reduced experimental variability could provide more definitive insights into the differences among the groups and elucidate the effects of DUSP6 knockout on extracellular dopamine levels. Additionally, as previous studies have reported that DUSP6 plays a role in stabilizing SLC6A3 (Mortensen et al., 2008), the observed increasing trend in dopamine levels is also speculated to be due to this stabilizing effect at the protein level. Therefore, future research is suggested to investigate the impact of DUSP6 on SLC6A3 protein expression in human dopaminergic neurons.

In conclusion, our study contributes to a deeper understanding of the molecular underpinnings of ADHD through the lens of GWAS confirmed risk gene. Further, it underscores the importance of *DUSP6* as a regulator of dopaminergic neurotransmission more generally. Future research should explore the downstream signalling pathways affected by *DUSP6* modulation and investigate the potential of targeting *DUSP6*-related pathways for therapeutic interventions in ADHD and related psychiatric disorders. Additionally, studies incorporating behavioural assessments and in vivo models could further elucidate the functional consequences of *DUSP6* alterations and validate its role as a critical modulator of neuropsychiatric health.

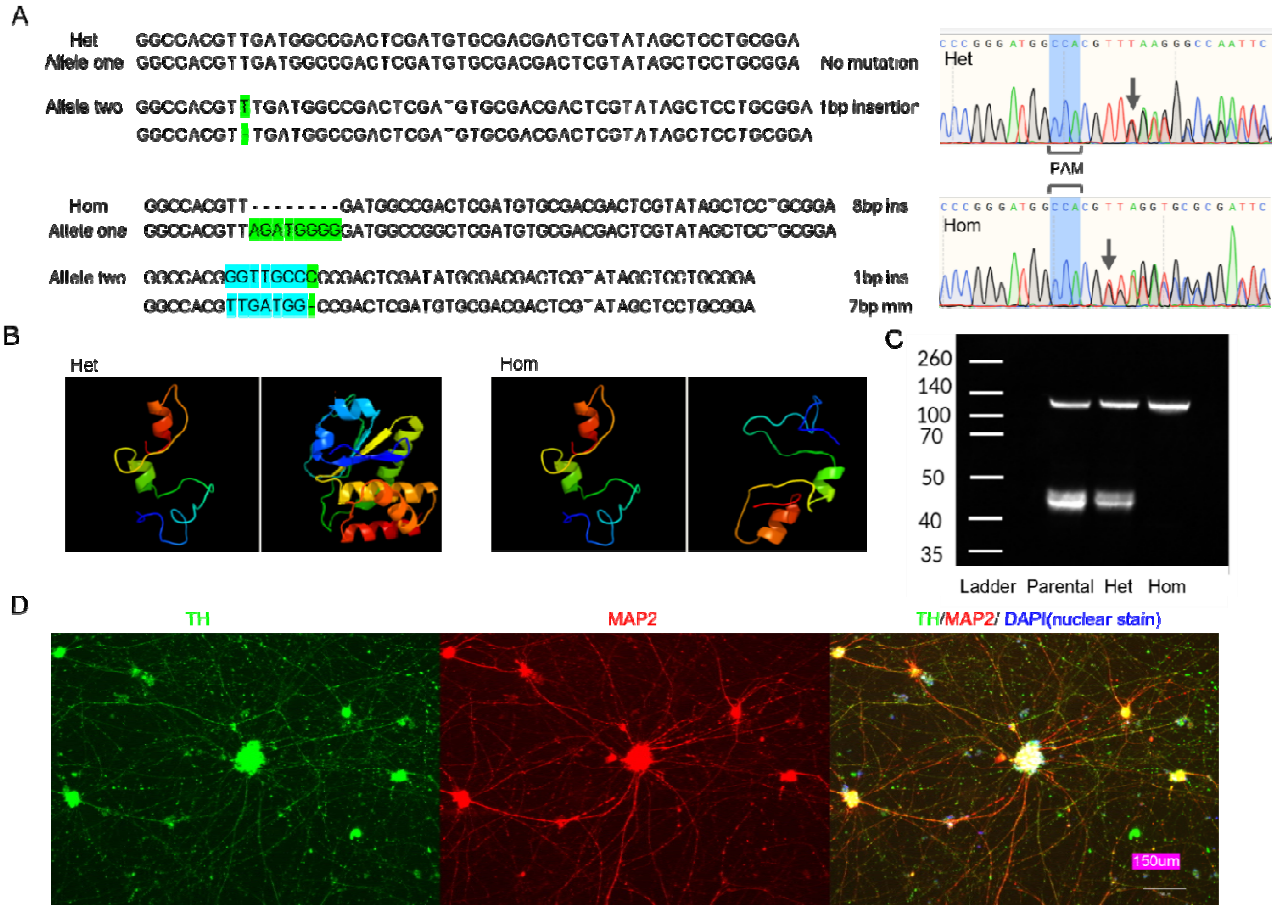

Figure 1. Generation of *DUSP6* knockout neuronal models. A) CRISPR-Cas9 editing generated two homogeneous single-cell iPSC clones: one Het and one Hom, as confirmed by Sanger sequencing. The Het line is characterized by a 1-base insertion in one allele, while the Hom line is characterized by a 1-base insertion in one allele and an 8-base insertion in the other allele of *DUSP6* exon one. **B)** PHYRE2 protein structure prediction tool revealed altered conformational structures in both the Het and Hom lines. **C)** Western blotting confirmed reduced DUSP6 protein expression in the Het and complete absence in the Hom lines in a dose-dependent manner. **D)** Immunocytochemical imaging of differentiated dopaminergic neurons derived from the iPSC lines shows a high purity of neurons expressing TH, MAP2 and DAPI nuclear stain.

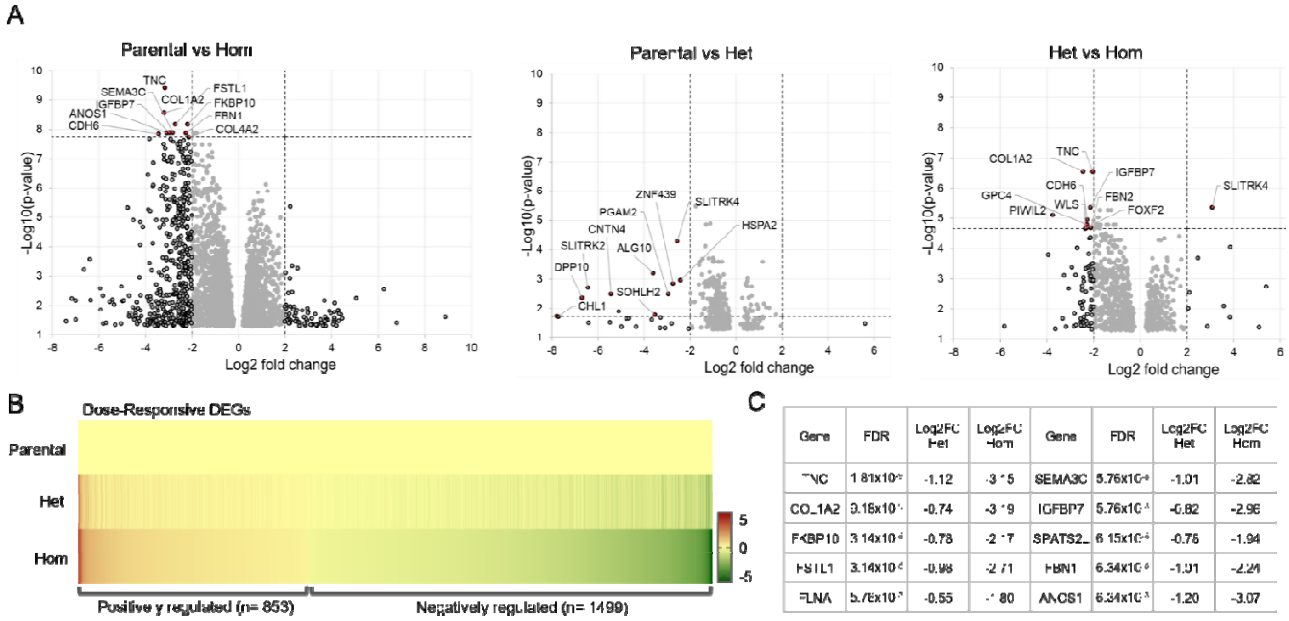

Gene	FDR	Log2FC Het	Log2FC Hom	Gene	FDR	Log2FC Het	Log2FC Hom
TNC	1.81x10[illegible]	-1.12	-3.[illegible]5	SEMA3C	5.76x10[illegible]	-1.01	-2.82
COL1A2	3.18x10[illegible]	-0.74	-3.[illegible]9	IGFBP7	5.76x10[illegible]	-0.82	-2.98
FKBP10	3.14x10[illegible]	-0.78	-2.[illegible]7	SPATS2_	6.15x10[illegible]	-0.75	-1.94
FSTL1	3.14x10[illegible]	-0.98	-2.71	FBN1	6.34x10[illegible]	-1.01	-2.24
FLNA	5.78x10[illegible]	-0.55	-[illegible]80	ANOS1	6.34x10[illegible]	-1.20	-3.07

Figure 2. Transcriptome analysis of knockout lines and biological clustering of DEGs. A) Volcano plot illustrating the pairwise comparison of *DUSP6* knockout DEGs across parental, Het, and Hom lines. The top 10 high-effect-size DEGs (log2FC ≥ 2), ranked by significance, are highlighted in red. **B)** Heat map displaying dose-responsive DEGs across parental, Het, and Hom lines. **C)** Table listing the top 10 dose-responsive DEGs, including their FDR and log2 fold change values.

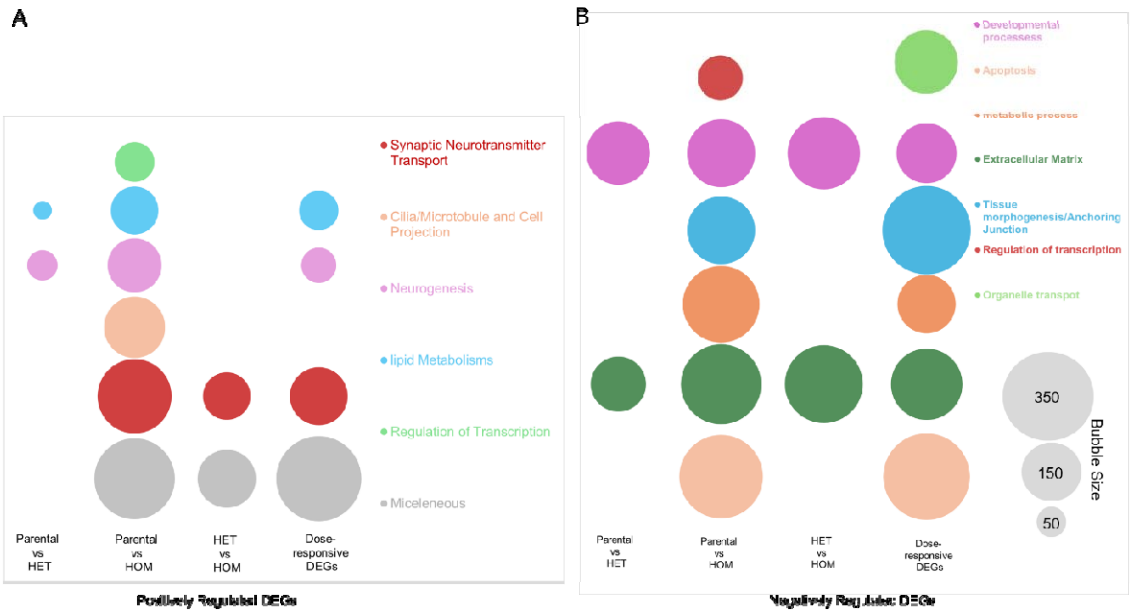

Figure 3. Biological clustering of DEGs. Bubble chart depicting the biological network clustering of **A)** positively and **B)** negatively regulated DEGs. The size of each circle corresponds to the number of genes in each cluster, while the colour represents specific clusters across groups.

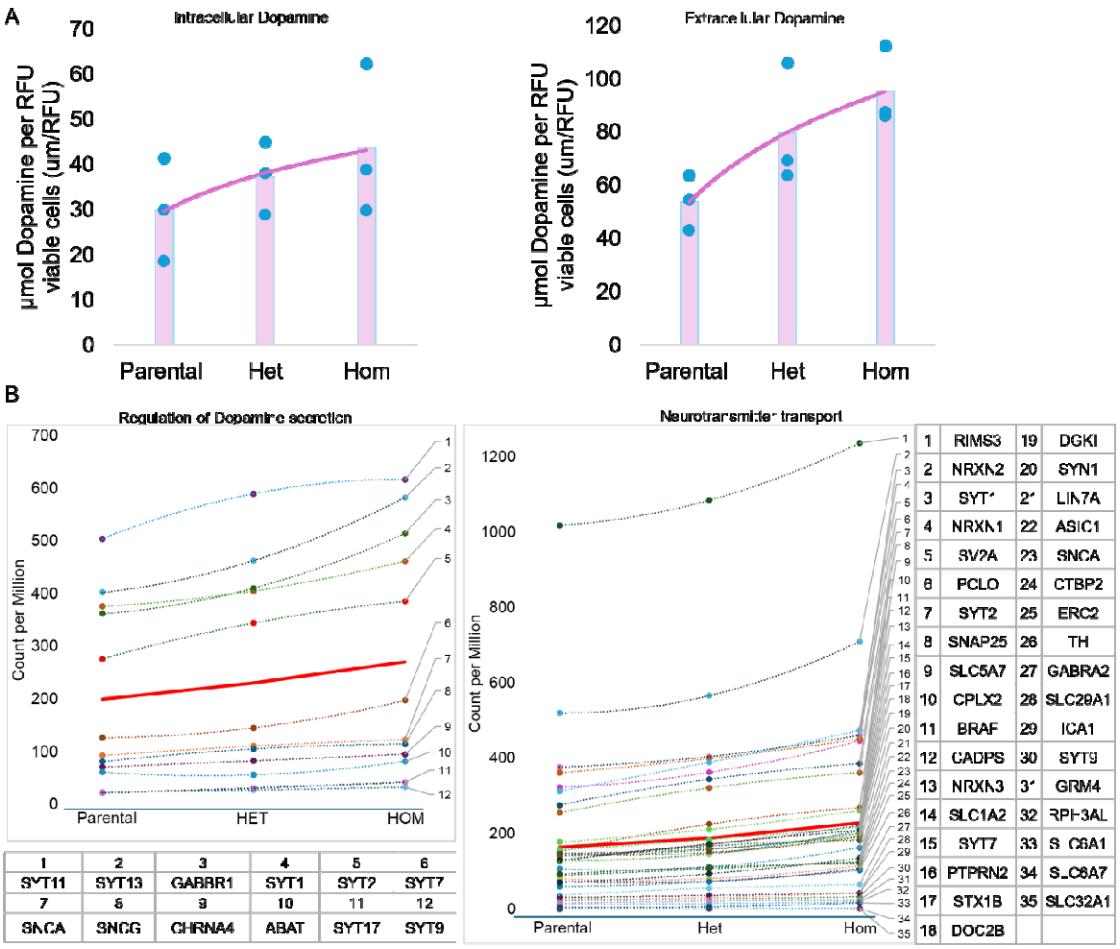

Figure 4. Dose-dependent regulatory effect of *DUSP6* on dopaminergic neurotransmission. A) ELISA measurements of dopamine concentrations show a trend of dose-dependent increase in dopamine level, with a significant increase in extracellular dopamine observed between the parental and Hom lines ($p = 0.016$), though it did not survive multiple comparison (p [illegible] 0.008). Bars represent the mean of dopamine concentration for each group **B)** Increasing expression trend across parental, Het, and Hom lines for DEGs that are involved in the biological processes of dopamine secretion (GO:0014059, FDR = 1.80×10^{-5}) and neurotransmitter transport (GO:0006836, FDR = 1.3×10^{-3}) derived from the parental vs. Hom comparison. The thick red line represents the trendline that best fits all data points.

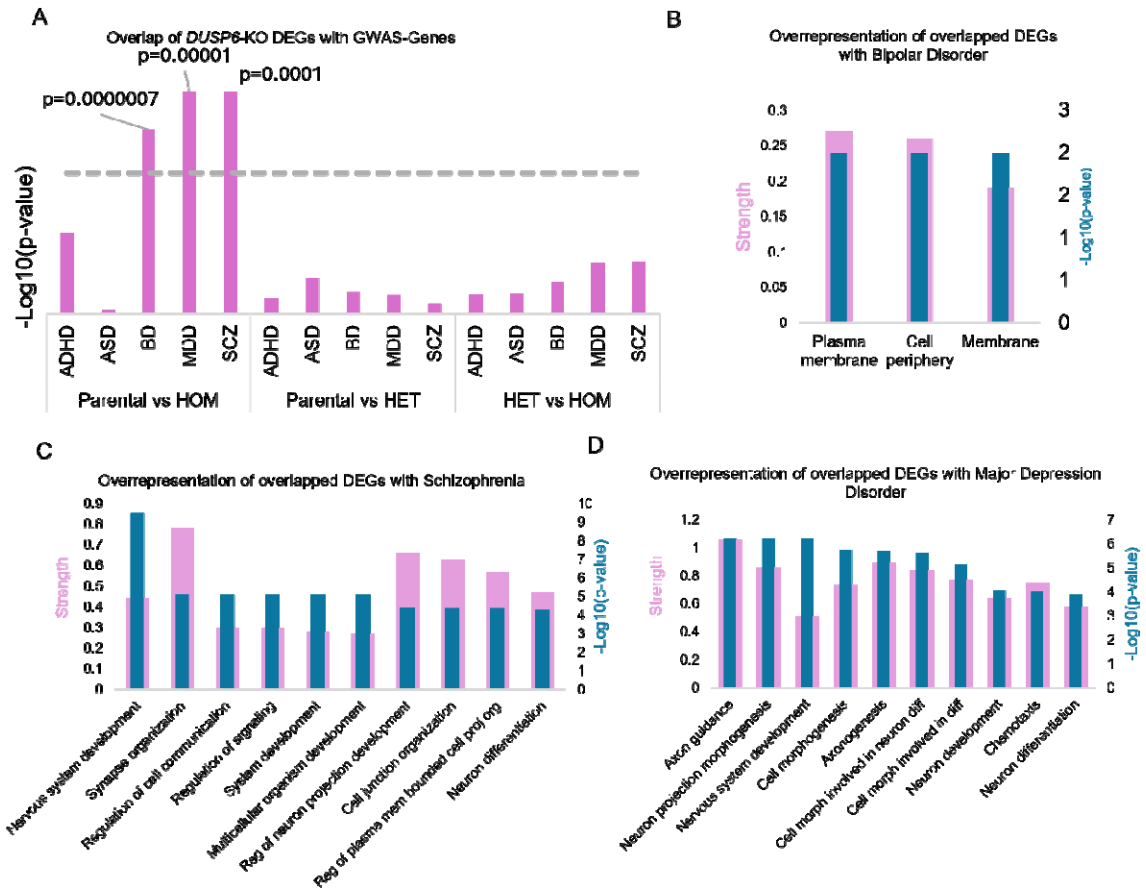

Figure 5. Overlap of *DUSP6*- knockout DEGs with GWAS-risk genes and enrichment analysis. A) *DUSP6* knockout DEGs show significant overlap with GWAS-identified risk genes for BD, MDD, and SCZ. **B)** Overrepresentation analysis of BP-overlapping DEGs reveals enrichment in biological processes, including membrane, plasma membrane and cell periphery. **C)** Top 10 biological processes, ranked by significance, identified through overrepresentation analysis of SCZ-overlapping DEGs. **D)** Top 10 biological processes, ranked by significance, identified through overrepresentation analysis of MDD-overlapping DEGs.

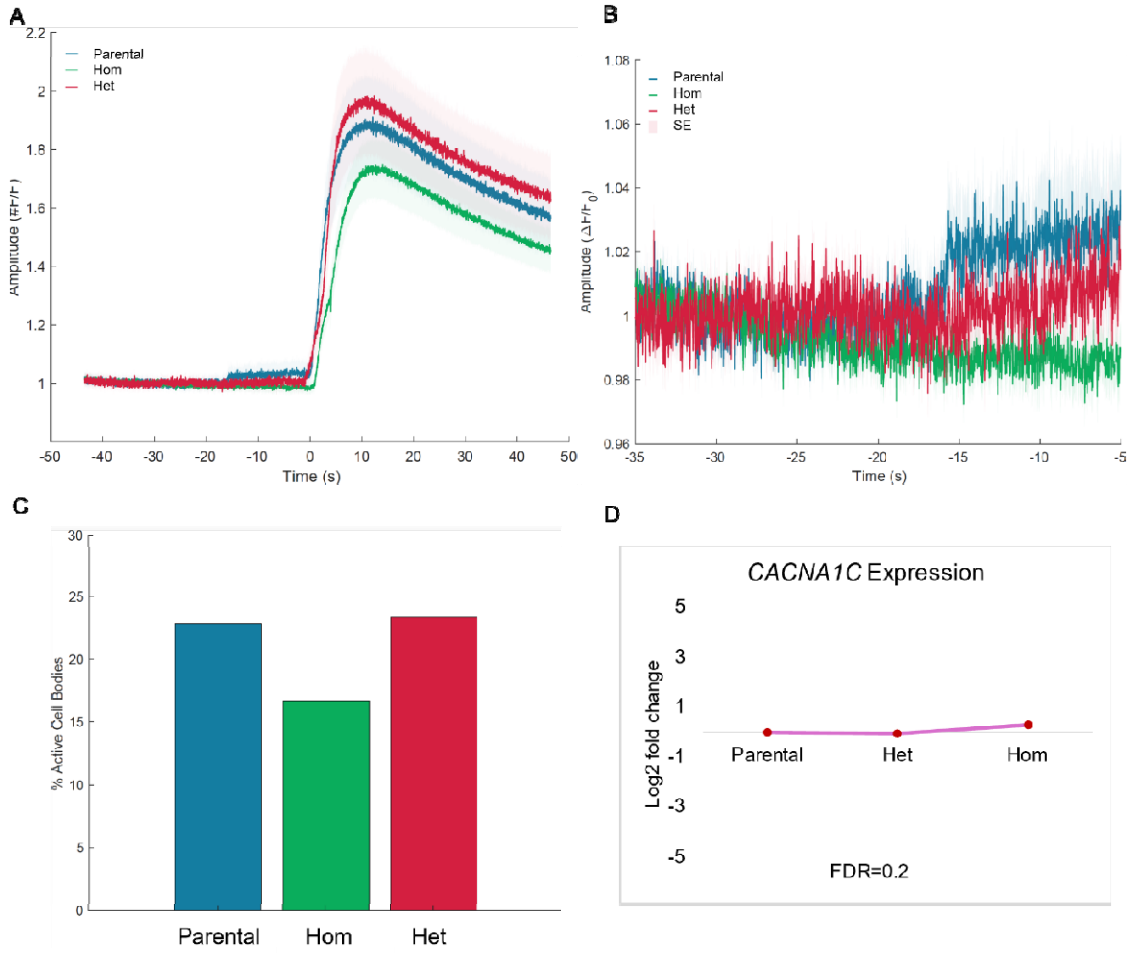

Figure 6. Effect of *DUSP6* knockout on *CACNA1C* calcium channel in dopaminergic neurons. Measurements of **A**) evoked and **B)** baseline amplitude show no significant differences across the parental, Het, and Hom lines. **C)** Similarly, no significant differences were observed in the frequency of spontaneously active cells across the lines. **D)** Consistently, RNA-sequencing results showed *CACNA1C* expression is not significantly altered due to the knockout of *DUSP6* in either the Het or Hom lines.

References

Alsanie, W. F., Penna, V., Schachner, M., Thompson, L. H., & Parish, C. L. (2017). Homophilic binding of the neural cell adhesion molecule CHL1 regulates development of ventral midbrain dopaminergic pathways. *Sci Rep, 7*(1), 9368. doi:10.1038/s41598-017-09599-y

Arora, S., Yeliosof, O., & Chin, V. L. (2023). A case of novel mutation in ANOS1 (KAL1) gene and review of Kallmann syndrome. *Endocrinol Diabetes Metab Case Rep, 2023*(2). doi:10.1530/EDM-22-0310

Barnes, A. M., Cabral, W. A., Weis, M., Makareeva, E., Mertz, E. L., Leikin, S., . . . Marini, J. C. (2012). Absence of FKBP10 in recessive type XI osteogenesis imperfecta leads to diminished collagen cross-linking and reduced collagen deposition in extracellular matrix. *Hum Mutat, 33*(11), 1589-1598. doi:10.1002/humu.22139

Brohee, S., & van Helden, J. (2006). Evaluation of clustering algorithms for protein-protein interaction networks. *BMC Bioinformatics, 7*, 488. doi:10.1186/1471-2105-7-488

Chen, L., Hui, L., & Li, J. (2024). The multifaceted role of insulin-like growth factor binding protein 7. *Front Cell Dev Biol, 12*, 1420862. doi:10.3389/fcell.2024.1420862

Chernousov, M. A., Baylor, K., Stahl, R. C., Stecker, M. M., Sakai, L. Y., Lee-Arteaga, S., . . . Carey, D. J. (2010). Fibrillin-2 is dispensable for peripheral nerve development, myelination and regeneration. *Matrix Biol, 29*(5), 357-368. doi:10.1016/j.matbio.2010.02.006

Clay, M. R., & Halloran, M. C. (2014). Cadherin 6 promotes neural crest cell detachment via F-actin regulation and influences active Rho distribution during epithelial-to-mesenchymal transition. *Development, 141*(12), 2506-2515. doi:10.1242/dev.105551

de Leeuw, C. A., Mooij, J. M., Heskes, T., & Posthuma, D. (2015). MAGMA: generalized gene-set analysis of GWAS data. *PLoS Comput Biol, 11*(4), e1004219. doi:10.1371/journal.pcbi.1004219

Demontis, D., Walters, G. B., Athanasiadis, G., Walters, R., Therrien, K., Nielsen, T. T., . . . Borglum, A. D. (2023). Genome-wide analyses of ADHD identify 27 risk loci, refine the genetic architecture and implicate several cognitive domains. *Nat Genet, 55*(2), 198-208. doi:10.1038/s41588-022-01285-8

Demontis, D., Walters, R. K., Martin, J., Mattheisen, M., Als, T. D., Agerbo, E., . . . Neale, B. M. (2019). Discovery of the first genome-wide significant risk loci for attention deficit/hyperactivity disorder. *Nat Genet, 51*(1), 63-75. doi:10.1038/s41588-018-0269-7

Dobin, A., Davis, C. A., Schlesinger, F., Drenkow, J., Zaleski, C., Jha, S., . . . Gingeras, T. R. (2013). STAR: ultrafast universal RNA-seq aligner. *Bioinformatics, 29*(1), 15-21. doi:10.1093/bioinformatics/bts635

Everson, J. L., Fink, D. M., Yoon, J. W., Leslie, E. J., Kietzman, H. W., Ansen-Wilson, L. J., . . . Lipinski, R. J. (2017). Sonic hedgehog regulation of Foxf2 promotes cranial neural crest mesenchyme proliferation and is disrupted in cleft lip morphogenesis. *Development, 144*(11), 2082-2091. doi:10.1242/dev.149930

Faraone, S. V., Bellgrove, M. A., Brikell, I., Cortese, S., Hartman, C. A., Hollis, C., . . . Buitelaar, J. K. (2024). Attention-deficit/hyperactivity disorder. *Nat Rev Dis Primers, 10*(1), 11. doi:10.1038/s41572-024-00495-0

Farhy-Tselnicker, I., van Casteren, A. C. M., Lee, A., Chang, V. T., Aricescu, A. R., & Allen, N. J. (2017). Astrocyte-Secreted Glypican 4 Regulates Release of Neuronal Pentraxin 1 from Axons to Induce Functional Synapse Formation. *Neuron, 96*(2), 428-445 e413. doi:10.1016/j.neuron.2017.09.053

Felix Krueger, F. J., Phil Ewels, Ebrahim Afyounian, & Benjamin Schuster-Boeckler . . (2021). FelixKrueger/TrimGalore: v0.6.7 - DOI via Zenodo (0.6.7). *Zenodo*. doi:https://doi.org/10.5281/zenodo.5127899

Gasperini, C., Tuntevski, K., Beatini, S., Pelizzoli, R., Lo Van, A., Mangoni, D., . . . De Pietri Tonelli, D. (2023). Piwil2 (Mili) sustains neurogenesis and prevents cellular senescence in the postnatal hippocampus. *EMBO Rep, 24*(2), e53801. doi:10.15252/embr.202153801

Gene Ontology, C., Aleksander, S. A., Balhoff, J., Carbon, S., Cherry, J. M., Drabkin, H. J., . . . Westerfield, M. (2023). The Gene Ontology knowledgebase in 2023. *Genetics, 224*(1). doi:10.1093/genetics/iyad031

Harshil Patel, P. E., Alexander Peltzer, Olga Botvinnik, Gregor Sturm, Denis Moreno, Pranathi Vemuri, silviamorins, Lorena Pantano, Mahesh Binzer-Panchal, nf-core bot, Gavin Kelly, Maxime U. Garcia, FriederikeHanssen, Matthias Zepper, James A. Fellows Yates, Chris Cheshire, rfenouil, Jose Espinosa-Carrasco, … George Hall. (2023). nf-core/rnaseq: nf-core/rnaseq v3.10.1 - Plastered Rhodium Rudolph (3.10.1). *Zenodo*. doi:https://doi.org/10.5281/zenodo.7505987

Hawi, Z., Tong, J., Dark, C., Yates, H., Johnson, B., & Bellgrove, M. A. (2018). The role of cadherin genes in five major psychiatric disorders: A literature update. *Am J Med Genet B Neuropsychiatr Genet, 177*(2), 168-180. doi:10.1002/ajmg.b.32592

Kelley, L. A., Mezulis, S., Yates, C. M., Wass, M. N., & Sternberg, M. J. (2015). The Phyre2 web portal for protein modeling, prediction and analysis. *Nat Protoc, 10*(6), 845-858. doi:10.1038/nprot.2015.053

Kondo, M. A., Norris, A. L., Yang, K., Cheshire, M., Newkirk, I., Chen, X., . . . Pevsner, J. (2022). Dysfunction of mitochondria and GABAergic interneurons in the anterior cingulate cortex of individuals with schizophrenia. *Neurosci Res, 185*, 67-72. doi:10.1016/j.neures.2022.09.011

Koudinov, A. R., & Koudinova, N. V. (2002). Cholesterol's role in synapse formation. *Science, 295*(5563), 2213. doi:10.1126/science.295.5563.2213a

Kumari, E., Xu, A., Chen, R., Yan, Y., Yang, Z., & Zhang, T. (2023). FSTL1-knockdown improves neural oscillation via decreasing neuronal-inflammation regulating apoptosis in Abeta(1-42) induced AD model mice. *Exp Neurol, 359*, 114231. doi:10.1016/j.expneurol.2022.114231

Labonte, B., Engmann, O., Purushothaman, I., Menard, C., Wang, J., Tan, C., . . . Nestler, E. J. (2017). Sex-specific transcriptional signatures in human depression. *Nat Med, 23*(9), 1102-1111. doi:10.1038/nm.4386

Law, C. W., Chen, Y., Shi, W., & Smyth, G. K. (2014). voom: Precision weights unlock linear model analysis tools for RNA-seq read counts. *Genome Biol, 15*(2), R29. doi:10.1186/gb-2014-15-2-r29

Linetti, A., Fratangeli, A., Taverna, E., Valnegri, P., Francolini, M., Cappello, V., . . . Rosa, P. (2010). Cholesterol reduction impairs exocytosis of synaptic vesicles. *J Cell Sci, 123*(Pt 4), 595-605. doi:10.1242/jcs.060681

Maffie, J., & Rudy, B. (2008). Weighing the evidence for a ternary protein complex mediating A-type K+ currents in neurons. *J Physiol, 586*(23), 5609-5623. doi:10.1113/jphysiol.2008.161620

Matsumoto, Y., Miwa, H., Katayama, K. I., Watanabe, A., Yamada, K., Ito, T., . . . Aruga, J. (2024). Slitrk4 is required for the development of inhibitory neurons in the fear memory circuit of the lateral amygdala. *Front Mol Neurosci, 17*, 1386924. doi:10.3389/fnmol.2024.1386924

Moreno-Flores, M. T., Martin-Aparicio, E., Martin-Bermejo, M. J., Agudo, M., McMahon, S., Avila, J., . . . Wandosell, F. (2003). Semaphorin 3C preserves survival and induces neuritogenesis of cerebellar granule neurons in culture. *J Neurochem, 87*(4), 879-890. doi:10.1046/j.1471-4159.2003.02051.x

Mortensen, O. V. (2013). MKP3 eliminates depolarization-dependent neurotransmitter release through downregulation of L-type calcium channel Cav1.2 expression. *Cell Calcium, 53*(3), 224-230. doi:10.1016/j.ceca.2012.12.004

Mortensen, O. V., Larsen, M. B., Prasad, B. M., & Amara, S. G. (2008). Genetic complementation screen identifies a mitogen-activated protein kinase phosphatase, MKP3, as a regulator of dopamine transporter trafficking. *Mol Biol Cell, 19*(7), 2818-2829. doi:10.1091/mbc.e07-09-0980

Namipashaki, A., Pugsley, K., Liu, X., Abrehart, K., Lim, S. M., Sun, G., . . . Hawi, Z. (2023). Integration of xeno-free single-cell cloning in CRISPR-mediated DNA editing of human iPSCs improves homogeneity and methodological efficiency of cellular disease modeling. *Stem Cell Reports, 18*(12), 2515-2527. doi:10.1016/j.stemcr.2023.10.013

Nowicka-Bauer, K., Malcher, A., Wloczkowska, O., Kamieniczna, M., Olszewska, M., & Kurpisz, M. K. (2022). Evaluation of seminal plasma HSPA2 protein as a biomarker of human spermatogenesis status. *Reprod Biol, 22*(1), 100597. doi:10.1016/j.repbio.2021.100597

Park, M., Lee, Y., Jang, H., Lee, O. H., Park, S. W., Kim, J. H., . . . Choi, Y. (2016). SOHLH2 is essential for synaptonemal complex formation during spermatogenesis in early postnatal mouse testes. *Sci Rep, 6*, 20980. doi:10.1038/srep20980

Patro, R., Duggal, G., Love, M. I., Irizarry, R. A., & Kingsford, C. (2017). Salmon provides fast and bias-aware quantification of transcript expression. *Nat Methods, 14*(4), 417-419. doi:10.1038/nmeth.4197

Patterson, K. I., Brummer, T., O'Brien, P. M., & Daly, R. J. (2009). Dual-specificity phosphatases: critical regulators with diverse cellular targets. *Biochem J, 418*(3), 475-489. doi:10.1042/bj20082234

Powell, S. K., O'Shea, C., Townsley, K., Prytkova, I., Dobrindt, K., Elahi, R., . . . Brennand, K. J. (2023). Induction of dopaminergic neurons for neuronal subtype-specific modeling of psychiatric disease risk. *Mol Psychiatry, 28*(5), 1970-1982. doi:10.1038/s41380-021-01273-0

Powell., D. (2019). drpowell/degust 4.1.1 (4.1.1). *Zenodo*. doi:https://doi.org/10.5281/zenodo.3501067

Prakash, N. (2022). Developmental pathways linked to the vulnerability of adult midbrain dopaminergic neurons to neurodegeneration. *Front Mol Neurosci, 15*, 1071731. doi:10.3389/fnmol.2022.1071731

Ramtekkar, U. P., Reiersen, A. M., Todorov, A. A., & Todd, R. D. (2010). Sex and age differences in attention-deficit/hyperactivity disorder symptoms and diagnoses: implications for DSM-V and ICD-11. *J Am Acad Child Adolesc Psychiatry, 49*(3), 217-228 e211-213. Retrieved from https://www.ncbi.nlm.nih.gov/pubmed/20410711

Sadick, J. S., O'Dea, M. R., Hasel, P., Dykstra, T., Faustin, A., & Liddelow, S. A. (2022). Astrocytes and oligodendrocytes undergo subtype-specific transcriptional changes in Alzheimer's disease. *Neuron, 110*(11), 1788-1805 e1710. doi:10.1016/j.neuron.2022.03.008

Seternes, O. M., Kidger, A. M., & Keyse, S. M. (2019). Dual-specificity MAP kinase phosphatases in health and disease. *Biochim Biophys Acta Mol Cell Res, 1866*(1), 124-143. doi:10.1016/j.bbamcr.2018.09.002

Sheen, V. L., Feng, Y., Graham, D., Takafuta, T., Shapiro, S. S., & Walsh, C. A. (2002). Filamin A and Filamin B are co-expressed within neurons during periods of neuronal migration and can physically interact. *Hum Mol Genet, 11*(23), 2845-2854. doi:10.1093/hmg/11.23.2845

Soneson, C., Love, M. I., & Robinson, M. D. (2015). Differential analyses for RNA-seq: transcript-level estimates improve gene-level inferences. *F1000Res, 4*, 1521. doi:10.12688/f1000research.7563.2

Struyf, J., Dobrin, S., & Page, D. (2008). Combining gene expression, demographic and clinical data in modeling disease: a case study of bipolar disorder and schizophrenia. *BMC Genomics, 9*, 531. doi:10.1186/1471-2164-9-531

Szklarczyk, D., Gable, A. L., Nastou, K. C., Lyon, D., Kirsch, R., Pyysalo, S., . . . von Mering, C. (2021). The STRING database in 2021: customizable protein-protein networks, and functional characterization of user-uploaded gene/measurement sets. *Nucleic Acids Res, 49*(D1), D605-D612. doi:10.1093/nar/gkaa1074

Szklarczyk, D., Kirsch, R., Koutrouli, M., Nastou, K., Mehryary, F., Hachilif, R., . . . von Mering, C. (2023). The STRING database in 2023: protein-protein association networks and functional enrichment analyses for any sequenced genome of interest. *Nucleic Acids Res, 51*(D1), D638-D646. doi:10.1093/nar/gkac1000

Tong, J., Lee, K. M., Liu, X., Nefzger, C. M., Vijayakumar, P., Hawi, Z., . . . Bellgrove, M. A. (2019). Generation of four iPSC lines from peripheral blood mononuclear cells (PBMCs) of an attention deficit hyperactivity disorder (ADHD) individual and a healthy sibling in an Australia-Caucasian family. *Stem Cell Res, 34*, 101353. doi:10.1016/j.scr.2018.11.014

Tucic, M., Stamenkovic, V., & Andjus, P. (2021). The Extracellular Matrix Glycoprotein Tenascin C and Adult Neurogenesis. *Front Cell Dev Biol, 9*, 674199. doi:10.3389/fcell.2021.674199

Yang, D., Wang, X., Zhang, L., Fang, Y., Zheng, Q., Liu, X., . . . Hua, F. (2022). Lipid metabolism and storage in neuroglia: role in brain development and neurodegenerative diseases. *Cell Biosci, 12*(1), 106. doi:10.1186/s13578-022-00828-0

Zagaglia, S., Selch, C., Nisevic, J. R., Mei, D., Michalak, Z., Hernandez-Hernandez, L., . . . Sisodiya, S. M. (2018). Neurologic phenotypes associated with COL4A1/2 mutations: Expanding the spectrum of disease. *Neurology, 91*(22), e2078-e2088. doi:10.1212/WNL.0000000000006567